JOURNAL OF MECHANICAL ENGINEERING AND SCIENCES (JMES)
ISSN: 2289-4659 e-ISSN: 2231-8380
VOL. 16, ISSUE 1, 8801 – 8810
DOI: https://doi.org/10.15282/jmes.16.1.2022.12.0695

ORIGINAL ARTICLE

Optimization on fishing net porosity of twin pontoon floating breakwater in waves

S.F. Abdullah[1], A. Fitriadhy[1]

[1] Program of Maritime Technology, Faculty of Ocean Engineering Technology and Informatics, Universiti Malaysia Terengganu, 21030, Kuala Terengganu, Terengganu, Malaysia.
Phone: +6096683393; Fax: +6096683393

ABSTRACT – Chaotic process in wave passing through pores on the attached fishing net between twin pontoons of floating breakwater (TPFB) may lead to several severe problems relating to the hydrodynamic performance of such coastal structure. In presence of relatively fine pores, the wave transmission coefficient (K_t) tends to diminish while the reflection coefficient (K_r) will likely increase, or vice versa for coarse ones. The circumstance requires a complete design optimization study into obtaining an optimum porosity. This paper presents optimization on the fishing net porosity (n) of TPFB using artificial intelligence (AI) model. Here, a multi-objective evolutionary algorithm with various genetic parameters is proposed to search for optimum n ratio through primarily minimizing transmission (K_t) and reflection coefficients (K_r) while maximizing energy dissipation coefficient (K_d). In addition, a computational fluid dynamic (CFD) programme is developed using an extended Reynolds Average Navier-Stokes (RANS) solver for a solid-permeable obstacle. Several parameters such as wavelengths and porosity ratios including a set of optimization criteria, have been taken into account in the simulation, where the optimum solution is then selected from various populations. Meanwhile, the optimum result will be qualitatively evaluated, in which it is visualized by the characteristic patterns of induced energy dissipation. The results revealed that the optimization algorithm is effectively capable of determining global trade-offs between K_t, K_r, and K_d. As compared to the existing model, K_t and K_r decrease to less than 0.85 and 0.42 respectively, whereas K_d was increased up to 0.34 resulting in optimum hydrodynamics of TPFB indicated by further enhancement in the rate of energy dissipation across TPFB entanglement. For validation, the numerical model can fairly simulate well on the hydrodynamics of structure.

ARTICLE HISTORY
Received: 24th Mar. 2021
Revised: 17th Nov. 2021
Accepted: 03rd Dec. 2021

KEYWORDS
Optimization; artificial intelligence algorithm; floating breakwaters; wave transmission; wave reflection; energy dissipation

INTRODUCTION

Floating breakwaters are engineering structures basically applied to protect ports and harbours from severe wave impact. Also, they can be an alternative measure for shoreline protection, as compared to conventional breakwaters considering the compatibility with the incoming wave energies [1]. Furthermore, floating breakwaters offer several advantages of application in terms of low capital cost, deeper water depth, flexibility as well allowing continuous refreshment of coastal water. In designing such coastal structures hence, integrated hydrodynamic modelling using numerical optimization method increasingly becomes necessary.

A limited number of specific research on the design optimization of floating breakwaters had been pursued by authors. For example; Elchahal et al. [2] studied the optimization on the structure and stability of pontoon floating breakwaters; Mahmuddin and Kashiwagi [3] carried out the optimised modelling on the arbitrary shape of a floating breakwater, and Elchahal et al. [4] applied search technique for the optimal layout of detached breakwaters in port. However, these single-objective optimization studies were mostly devoted to restricting the wave transmission, K_t. While many severe environmental problems are often related to installed structures (e.g. seawalls and breakwaters), for instance; abnormal reflected waves, exacerbated coastal erosion etc. Therefore, a complete optimization problem with respect to wave reflection, K_r and energy dissipation K_d are appropriately considered and indicated as the main contribution in this study.

Over the years, various types of artificial intelligence (AI) models have appeared and have been extensively investigated in literature especially for marine applications such as adaptive neuro-fuzzy inference system (ANFIS) network [5-7], particle swarm optimization [8-9] including extensions of ordinary AI computation [10-11]. Nevertheless, the genetic algorithm (GA) remains the most robust intuitive search technique for multiple objective problems since it uses evolutionary parameters, namely, cross over and mutation, which firmly improves the initial points of solutions from local to globally optimal solutions. Moreover, the resulting solution is often optimum or near to optimum over an appropriate time.

This paper presents optimization on the fishing net porosity, n of twin pontoon floating breakwater (TPFB) using computational fluid dynamic (CFD) and artificial intelligence (AI) model approaches. Here, a multi-objective genetic algorithm is proposed to primarily minimize wave transmission (K_t), and reflection (K_r) coefficients, while maximizing the energy dissipation coefficient (K_d). Meanwhile, the CFD model is based on the extended Reynolds Average Navier-Stokes (RANS) solver for a solid-permeable obstacle. A series of parametric studies on various n ratios and wavelengths

*CORRESPONDING AUTHOR | S. F. Abdullah | ✉ sfakhruradzi@gmail.com

are numerically investigated, where the moored floating breakwater is analysed in three motional degrees of freedom which include surge, heave and pitch motions. In addition, a set of artificial intelligence algorithms of optimization objectives including boundary limits and criteria have been developed and then considered completely in the GA computation. For verification of the optimum result, the CFD model is employed to capture the characteristic patterns of induced energy dissipation across TPFB entanglement. Prior to optimization, numerical validation with the published experimental data in literature was also carried out, where the results agree fairly well with measurements.

OPTIMIZATION METHOD

Classically, in engineering design, the evaluation of the performance of a floating breakwater is based on ordinary calculation problems using conventional approaches such as experimental and theoretical analyses. The problem has not usually been seen as a complete design optimization problem. As a consequence, severe problems related to the structural efficiency of the installed breakwater cannot totally be eliminated.

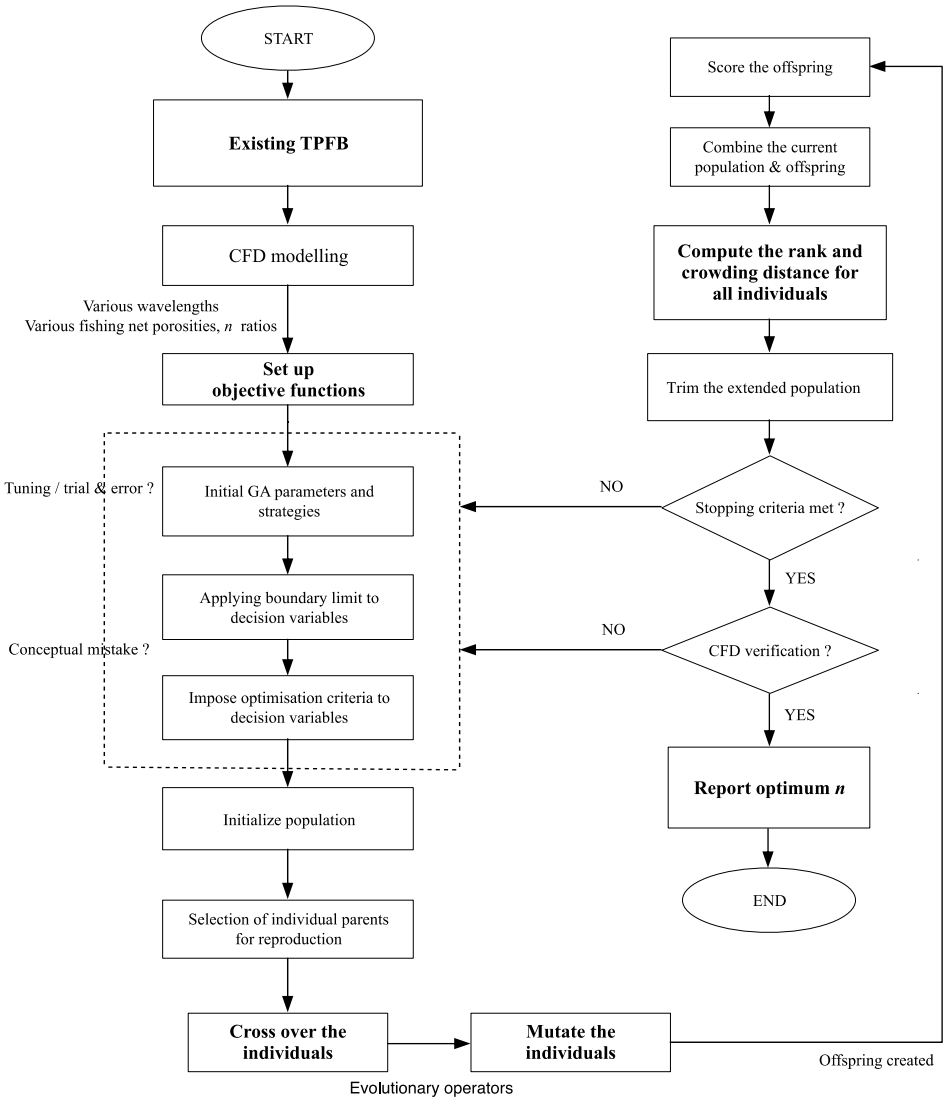

Figure 1. Optimization procedure

TPFB Definition

Figure 1 presents the optimization procedure applied in the present study to evaluate the performance of TPFB with respect to wave hydrodynamics. The CFD model was firstly used to validate the existing TPFB. In order to derive the pertinent objective functions, a series of parametric analyses were carried out on the wave interaction with TPFB under various wavelengths as well several fishing net porosities to produce significant results of K_t, K_r and K_d. Here, three porosity values corresponding to fine (0.3), medium (0.5) and coarse (0.6) are initially selected and then analyzed in the numerical model. In addition, Table 1 depicts the details on the environmental tested conditions. The definition of a wave−TPFB problem is deliberately established using mathematical expressions derived from the original relationships between the amplitude of the incident wave (A_i), reflected wave (A_r) and transmitted wave (A_t), as follows:

$$K_t = A_t/A_i \tag{1}$$

$$K_r = A_r/A_i \tag{2}$$

$$K_d = \sqrt{1 - {K_t}^2 - {K_r}^2} \tag{3}$$

Table 1. Parametric study

Wave height, H (m)	0.10, 0.125, 0.15, 0.175, 0.20
Wave period, T (s)	0.9, 1.0, 1.1, 1.2, 1.3, 1.4, 1.5, 1.6, 1.7, 1.8, 1.9, 2.0, 2.1

Fishing Net Algorithm

Creativity in the setting of mathematical rules is fundamental for GA calculations to obtain a realistic result. The objective functions are now assembled into the optimization algorithm which is formulated in the following form.

Find Y_x which:

$$\textit{Minimize} \qquad f_1(Y_x) = C_{1,1}{Y_x}^{C_{1,2}} - C_{1,3}Y_x + C_{1,4} \tag{4}$$

$$\textit{Maximize} \qquad f_2(Y_x) = C_{2,1}{Y_x}^{C_{2,2}} \tag{5}$$

$$\textit{Minimize} \qquad f_3(Y_x) = -C_{3,1}{Y_x}^{C_{3,2}} + C_{3,3}Y_x + C_{3,4} \tag{6}$$

where, $f_i(Y_x)$, $i = 1, 2, \dots, n$ are the objective functions corresponding to K_t, K_d and K_r for the decision variable, Y_x with variable coefficients, $C_{i,k}$, $k = 1, 2, \dots, n$. Referring to expressions (4) to (6), the applied problem of the floating breakwater was reduced to solving systems of nonlinear algebraic equations. And, a genetic algorithm is employed to perform a standard minimization or maximization procedure to find an optimum porosity of fishing net.

Wave-structure Constraint

A complete optimization algorithm is done by imposing a boundary limit and several criteria on the hydrodynamics for the design variable, as follows:

$$0.3 \leq Y_x \leq 0.6 \tag{7}$$

$$g(Y_x) \leq f_1 + 0.3 \tag{8}$$

$$b(Y_x) \geq f_2 + 0.8 \tag{9}$$

$$E(Y_x) = 1.0 - \sum_{i}^{n} f_i \tag{10}$$

In Eq. (7) the lower and upper variable bounds for the Y_x in search space is defined, which refers to fishing net porosity. Eqs. (8) and (9) present hydrodynamic criterions for TPFB corresponding to the requirements on wave attenuation and energy dissipation respectively. Additionally, all computed solutions must satisfy the energy equilibrium equation (Eq. (10)), formulated to ensure a realistic algorithm search.

Solution Approach

The process of solving and satisfying Eqs. (4)–(10) begins with the creation of offspring population over multiple generations using evolutionary operators; cross over and mutation (see Figure 1). The children are then scored by calculating their objective function values and feasibility. Besides that, the current population and the children are firmly combined into one matrix with different non-domination classes and diversities, where the rank and crowding distance for all individuals are appropriately computed. This solution comprising numerous populations of individual *n* has been created and revaluated with respect to defining constraints. The optimum solution is then chosen from a set of non-dominated fronts once a convergence iterating over 2–4 steps as well over various populations. Finally, the CFD simulation is carried out to visualize the induced energy dissipation due to presence of the optimum porosity. The establishment of this GA–CFD model associated with hydrodynamics is shown as overall study contribution.

NUMERICAL MODEL

The computational fluid dynamic (CFD) model is deliberately developed for hydrodynamic approximations of the moored floating breakwater. The descriptions of the numerical model are appropriately presented in the following subsections.

Two-dimensional Fluid Flow Algorithm

The Reynolds Average Navier-Stokes (RANS) equations coupled with $k-\varepsilon$ turbulence closure model and the volume of fluid (VOF) method are applied as the governing equations of fluid flow. The continuity and momentum conservation equations are formulated as:

$$\frac{\partial \theta \gamma_x u}{\partial x} + \frac{\partial \theta \gamma_y v}{\partial y} = 0 \tag{11}$$

$$\lambda_v \frac{\partial \theta u}{\partial t} + \lambda_x \theta u \frac{\partial \theta u}{\partial x} + \lambda_y \theta v \frac{\partial \theta v}{\partial y} = -\frac{\gamma_v}{\rho}\frac{\partial \theta p}{\partial x} + \theta \frac{\partial}{\partial x}\left[\gamma_x 2(\nu + \nu_t)\frac{\partial \theta u}{\partial x}\right] + \theta \frac{\partial}{\partial y}\left[\gamma_y \nu \left(\frac{\partial \theta u}{\partial y} + \frac{\partial \theta u}{\partial x}\right)\right] - R_x \tag{12}$$

$$\begin{aligned}\lambda_v \frac{\partial \theta v}{\partial t} + \lambda_x \theta u \frac{\partial \theta v}{\partial x} + \lambda_y \theta v \frac{\partial \theta v}{\partial y} \\ = -\frac{\gamma_v}{\rho}\frac{\partial \theta p}{\partial y} + \theta \frac{\partial}{\partial y}\left[\gamma_y 2(\nu + \nu_t)\frac{\partial \theta v}{\partial y}\right] + \theta \frac{\partial}{\partial x}\left[\gamma_x \nu \left(\frac{\partial \theta v}{\partial x} + \frac{\partial \theta u}{\partial y}\right)\right] - \gamma_v - R_y\end{aligned} \tag{13}$$

Velocity components u and v are in the Cartesian coordinate directions $x-y$. Gravitational acceleration is denoted by g, θ is partial treatment variable, ν is coefficient of kinematic viscosity and ν_t is fluid turbulent viscosity. Fluid density is denoted by ρ, and p represents the fluid pressure; γ_v is volume porosity; γ_x and γ_y are the surface porosities that represent the ratio of porous area to the sectional area of the cell surface. The parameters λ_v, λ_x and λ_y are defined from γ_v, γ_x and γ_y, respectively as $\lambda = \gamma + (1-\gamma)C_m$, where C_m is the inertia coefficient. The R_x and R_y are the drag force components in the $x-y$ direction. The transport equations of turbulence kinetic energy, k, and the dissipation rate of turbulent energy, ε, are defined as follows:

$$\frac{\partial \theta k}{\partial t} + \theta u \frac{\partial \theta k}{\partial x} + \theta v \frac{\partial \theta k}{\partial y} = \frac{\partial}{\partial x}\left[\left(\nu + \frac{\nu_t}{\sigma_k}\right)\frac{\partial \theta k}{\partial x}\right] + \frac{\partial}{\partial y}\left[\left(\nu + \frac{\nu_t}{\sigma_k}\right)\frac{\partial \theta k}{\partial y}\right] P_r - \varepsilon \tag{14}$$

$$\frac{\partial \theta \varepsilon}{\partial t} + \theta u \frac{\partial \theta \varepsilon}{\partial x} + \theta v \frac{\partial \theta \varepsilon}{\partial y} = \frac{\partial}{\partial x}\left[\left(\nu + \frac{\nu_t}{\sigma_\varepsilon}\right)\frac{\partial \theta \varepsilon}{\partial x}\right] + \frac{\partial}{\partial y}\left[\left(\nu + \frac{\nu_t}{\sigma_\varepsilon}\right)\frac{\partial \theta \varepsilon}{\partial y}\right] + C_{\varepsilon 1}(P_r)\frac{\varepsilon}{k} - C_{\varepsilon 2}\frac{\varepsilon}{k} \tag{15}$$

$$P_r = \nu_t\left[2\left(\frac{\partial \theta u}{\partial x}\right)^2 + 2\left(\frac{\partial \theta v}{\partial y}\right)^2 + \left(\frac{\partial \theta u}{\partial y} + \frac{\partial \theta v}{\partial x}\right)^2\right]; \qquad \nu_t = C_d \frac{k^2}{\varepsilon} \tag{16}$$

where C_d, $C_{\varepsilon 1}$, $C_{\varepsilon 2}$, σ_k and σ_ε are the model constants. The transport equation for the solution of the volume fraction of fluid, F is given as:

$$\frac{\partial(\gamma_v F)}{\partial t} + \frac{\partial(\gamma_x u F)}{\partial x} + \frac{\partial(\gamma_y v F)}{\partial y} = 0 \tag{17}$$

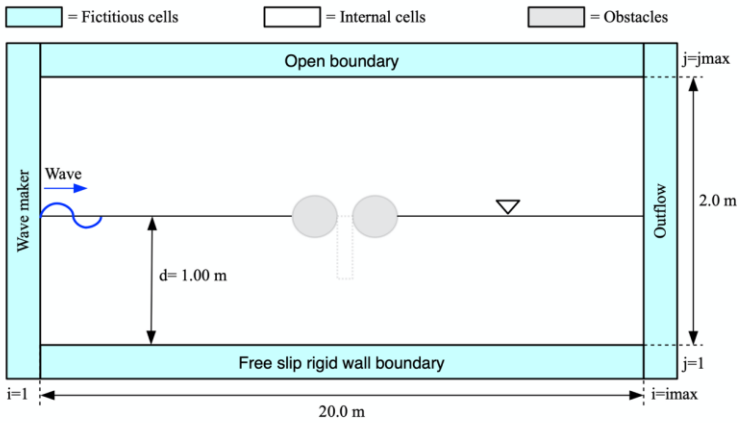

Figure 2. Computational domain

Boundary Conditions

Figure 2 shows the assigned boundary conditions for the computational domain including the internal obstacle of TPFB model. In accordance with the data of existing TPFB in literature, the geometrical similarity scale of 1:20 is selected for the present model. The geometrical and structural characteristics of the breakwater model are presented in Table 2. On the inflow boundary, the Dirichlet- type boundary condition is used to generate the wave into the domain. Additionally, the weakly-reflecting boundary condition is applied to this boundary and to the outflow boundary to reduce intermixing of the unphysical reflected waves. Further, in the internal obstacle boundary, the non-slip boundary condition for velocities, pressures and fluid fraction is properly applied. At the bottom boundary, the free-slip rigid wall is taken as the boundary condition, while the open boundary condition is applied for the top. Besides at the free surface, the turbulence boundary conditions are assumed with zero vertical fluxes of k and ε.

Table 2. TPFB structure particular

Characteristics			Value
Descriptions		Unit	
Length	$\boldsymbol{l}$	**m**	**0.760**
Width	$\boldsymbol{W}$	**m**	**0.500**
Height	$\boldsymbol{D}$	**m**	**0.510**
Draft	$\boldsymbol{d}$	**m**	**0.410**
Mass	$\boldsymbol{m}$	**kg**	**20.82**
Roll inertia	$\boldsymbol{I_{xx}}$	**kg*m^2**	**3.870**
Pitch inertia	$\boldsymbol{I_{yy}}$	**kg*m^2**	**7.370**
Yaw inertia	$\boldsymbol{I_{zz}}$	**kg*m^2**	**4.610**
Initial mass centre location	$\boldsymbol{C_g}$	**m**	**0.400**
Under keel clearance	**U.K.C**	**m**	**0.600**

Computational Procedure

The partial differential equations from Eqs. (11) to (17)) were numerically solved to obtain the solution of the unknown variables of u, v, p, F, k, ε. Here, the finite difference method is used and the time evolution of the unknown variables was advanced based on the Simple Implicit Method for Pressure-Linked Equations (SIMPLE) algorithm. For one computational cycle, the fluid flow algorithm computes and updates the pressure, velocities, turbulence fields and fluid fraction for each cell. The calculated F-values were then used to reconstruct the free surface. In the meantime, the boundary conditions are applied periodically in the domain. The algorithm runs the procedure again for new and next cycles until the simulation exceeds the total computational time.

RESULTS AND DISCUSSION

Figures 3 to 9 show the results of numerical modelling and optimization algorithm are successfully computed in this study. The discussions are focused on the verification of the CFD numerical model, hydrodynamic performance, and the elaboration on the optimization result. The pertaining discussions are appropriately presented in the following subsections.

CFD Verification

The mesh convergence study was properly carried out to estimate the convergence uncertainty of CFD simulation on the result of hydrodynamic coefficient. It should be noted here that the verification procedure was properly followed according to the manual of the 28th International Towing Tank Conference (ITTC (2017)) [12]. The transmission coefficients were calculated using total numbers of coarse (224), medium (334), and fine (444) cell meshing corresponding to the respective solutions $S_{i,3}$, $S_{i,2}$, and $S_{i,1}$, as shown in Table 3.

The result shows that the computational uncertainty for the medium mesh under monotonous convergence (R_i<1) is estimated to be -6.65%. Clearly, the medium resolution is sufficient to enable efficient CFD simulation. Thus, the total number of 334 meshing cells was adopted for all simulations since further increments of total cells was unnecessary on account of its insignificant influence on the result of the transmission coefficient.

Table 3. Uncertainty analysis for CFD verification

Parameter	Value
Solution of fine, $S_{i,1}$ (K_t)	0.720
Solution of medium, $S_{i,2}$ (K_t)	0.743
Solution of coarse, $S_{i,3}$ (K_t)	0.798
Convergence ratio, R_i	0.418
Order of accuracy, P_i	2.516
Extrapolated value, $S_{ext}^{3,2}$	0.704
Approximate error, δ_{app}^{*}	-7.4 %
Extrapolated error, δ_{ext}^{*}	-5.5 %
Convergence index, $CGI_{3,2}$	-6.65 %

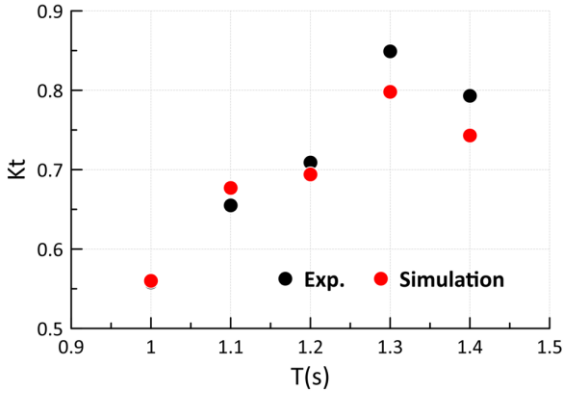

Figure 3. Transmission coefficient

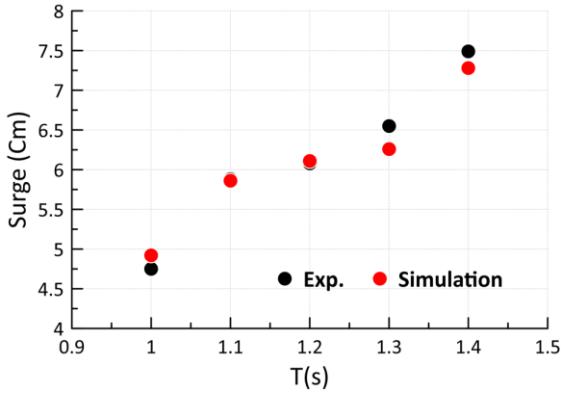

Figure 4. Surge response

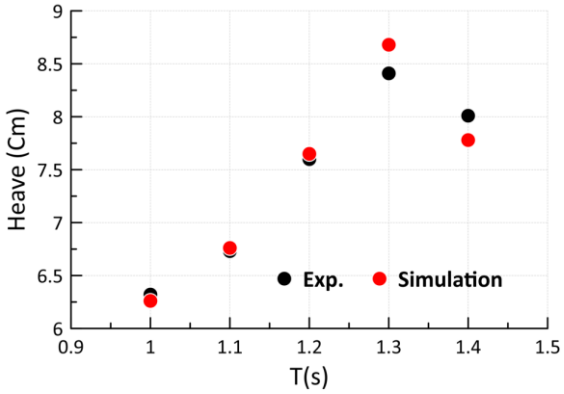

Figure 5. Heave response

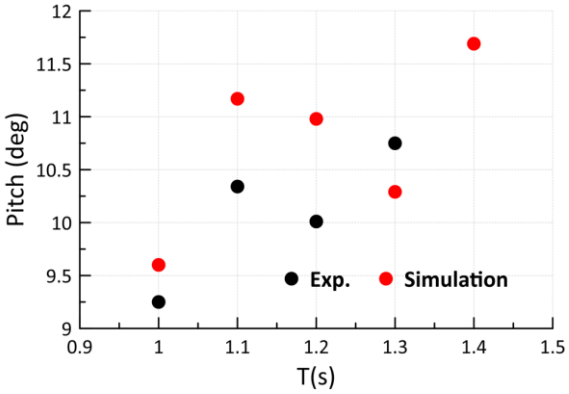

Figure 6. Pitch response

Hydrodynamic Performance of Existing TPFB Model

It is at first necessary to undertake a preliminary investigation and comparative survey towards the design optimization. Following the similar breakwater structure, the numerical results on the hydrodynamic performance of TPFB were compared to measurements by Ji et al. [13]. Figure 3 shows the changes of K_t with various wave periods for H = 0.20 m. While, Figures 4, 5 and 6 depict the motion responses of the floating breakwater. The results generally show qualitative and quantitative agreements were obtained between CFD model and the experimental results, in which the result discrepancies are approximately from 0.10% to 8.80%. A possible reason for this acceptable prediction can be dedicated to the effect of nonlinear effects on the interaction between wave and the floating breakwater.

The numerical results of surge and heave motions agree very well with measurements. With increasing wave kinetic energy the magnitudes of surge and heave markedly increase excepting for heaving mode beyond T = 1.3 s. This result is also supported on the declining trend of K_t in Figure 3. On the other hand, the pitch result exhibits a slight fluctuation for the whole range of wave period considered. Nevertheless, the result show a consistency in the data obtained from numerical approximations with measurements.

Besides that, it is worth to note that the CFD model can simulate very well the wave attenuating effect of TPFB at T = 1.4 s similar to the experimental counterpart, as shown in Figure 3. One of the reasons is because of the increased viscous and inertial drag damping due to increasing flow rate of water across the fishing net. This is proportional to the

drop amount of pressure and thus wave energy. The effect of enhancing this wave energy dissipation hydrodynamically reduces the wave crest and transmission on the leeward side of structure.

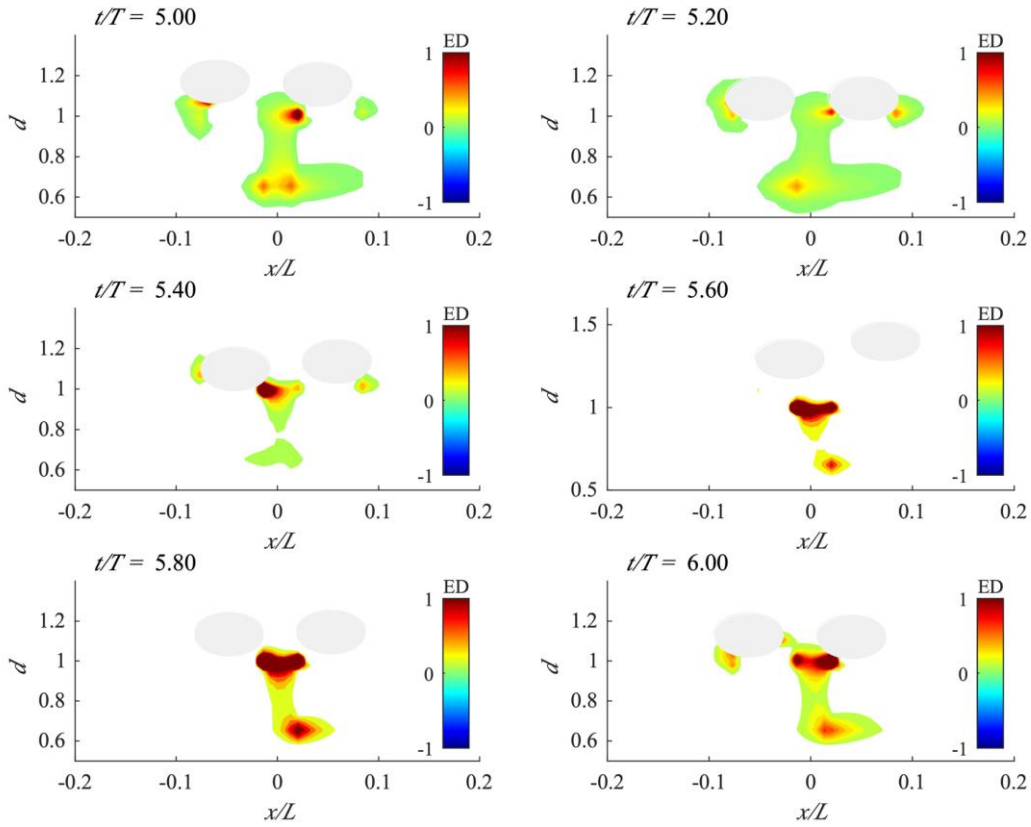

Figure 7. Instantaneous position of existing TPFB in a characteristic pattern of energy dissipation for one wave cycle (T = 1.4 s)

It is primarily observed that the reductions of K_t and heave motion beyond T = 1.3 s is basically due to the nonlinear phenomena such as wave breaking, overtopping, and increased drag friction across fishing net boundary, as supported in Figure 7. At t/T = 5.00 and 5.20, the friction effects from the wave run up and overtopped water are markedly observed on the pontoons as the incident wave approaching the floating breakwater. At the same time, the viscous friction and drag from fishing net is initially developed with mild green-yellow-red scaled colour energy dissipation. Here, the floating breakwater moves slightly towards negative magnitudes of surge and pitch (towards left and counter-clockwise direction), whereas with positive heave (upwards).

Beyond these wave cycles, the energy dissipation develops dramatically up to t/T = 5.80 due to the developed plunging wave breaking between twin pontoons as well increasing water particle velocity passing into the fishing net entanglement. The undulated trend of motions can be observed in the wave cycle captures, where the maximum positive magnitudes of surge, heave and pitch are recorded at t/T = 5.60. Just after the wave breaking phenomenon, the dissipations of wave run up and overtopping effects appear again at t/T = 6.00, and simultaneously reducing all the modes of breakwater motion. At the end of wave cycle, the distribution of energy dissipation at the inner and rear portions of the floating breakwater is significantly increased resulted from the wave overtopping and drag forces as indicated by the intense red-yellow scaled colours.

In conclusion, the numerical model can fairly simulate and reproduce many complex-nonlinear phenomena on the hydrodynamics of floating breakwater in waves. In particular, this investigation reveals that the relative breakwater draught (h/H > 2.00) is mostly effective at reducing K_t particularly in high amplitude waves. However, the design optimization on the fishing net porosity, n is necessarily required to enhance the energy dissipation, K_d that ultimately reducing K_t.

Optimization Result

The artificial intelligence algorithm was run to search for optimum fishing net porosity, n using various genetic parameters and strategies; 200 populations and various generations; simulated binary crossover, ρ_c = 0.9; crossover distribution index η_c = 20; polynomial mutation, ρ_m = 0.5 and distribution index of η_m = 20. Figure 8 presents the entire competing trade-offs considered in the optimization problem of n, projecting all non-dominated solutions evaluated in a

three-dimensional space between the design objectives specified: minimize wave transmission, K_t, maximize trade-off energy dissipation, K_d and minimize reflection coefficient, K_r. The result has convex and connected solutions.

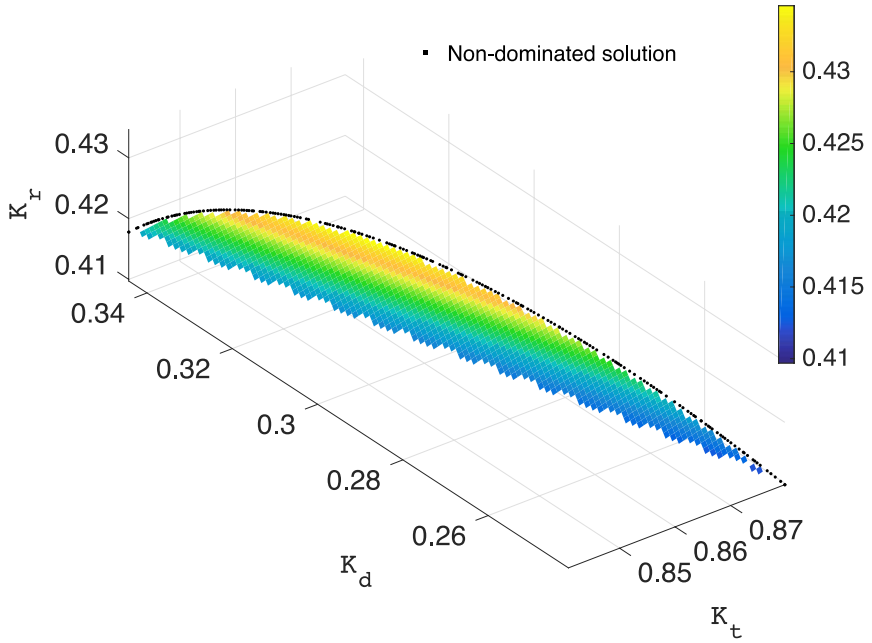

Figure 8. Non-dominated solutions of all objective functions for fishing net porosity

It is clear in Figure 8 that the non-dominated solutions consistently comprise a Pareto front and thus globally optimal trade-offs are found in this research. Based on the performance graph of individuals on the Pareto frontier, the average distance measure between individuals is obviously very small with an average convergence, Y (convergence metric) approximately 0.00022968. Meanwhile, the spread measure, Δ (diversity metric) of the Pareto front is approximately 0.162735. In fact, smaller value of these performance measures indicates a high performance result is obtained. Referring to an extreme solution in Figure 8, the resulting optimum n is equal to 0.557. For this n ratio, K_d increased up to 0.34, whereas K_t and K_r decreased to less than 0.85 and 0.42 respectively.

However, when this resulting optimum porosity is equal to 0.557 the optimization criteria in Eqs. (8) to (9) are still cannot be satisfied since the values of K_t and K_r are greater than 0.3 while K_d is less than 0.5. Fitriadhy et *al*. [14] found that a prominent optimization effect of the lateral separation between twin pontoons on the attribute in attenuating amounts of K_t and K_r. Nonetheless, in similar to Fitriadhy et al. [14], the results generally reveal a consistency on the reduction and enhancement in the attribute of K_t and K_d confirmed by the mathematical expressions derived in Eqs. (4) and (5). This is inherently due to increased wave absorbing effects of optimized n of TPFB especially in longer waves related to the augmented effect on K_d. A reason behind this hydrodynamic effect is due to the nonlinear phenomena of increasing wave energy passing through the optimized pores on the fishing net, as shown in Figure 9.

In comparison to existing TPFB (see Figure 7), the characteristic pattern of turbulence energy dissipation across the optimum fishing-net breakwater and at the rear portion is more develop and intense, as depicted by the green-yellow-red scaled colour contours. Moreover, the motional amplitudes of surge, heave and pitch modes can be seen to slightly damped for a complete wave cycle, inherently due to wave absorbing effect. A reason behind this motional behaviour is due to the augmented damping effects from wave trapping and induced turbulence energy apart from increased drag friction and flow reversal across the netting entanglement.

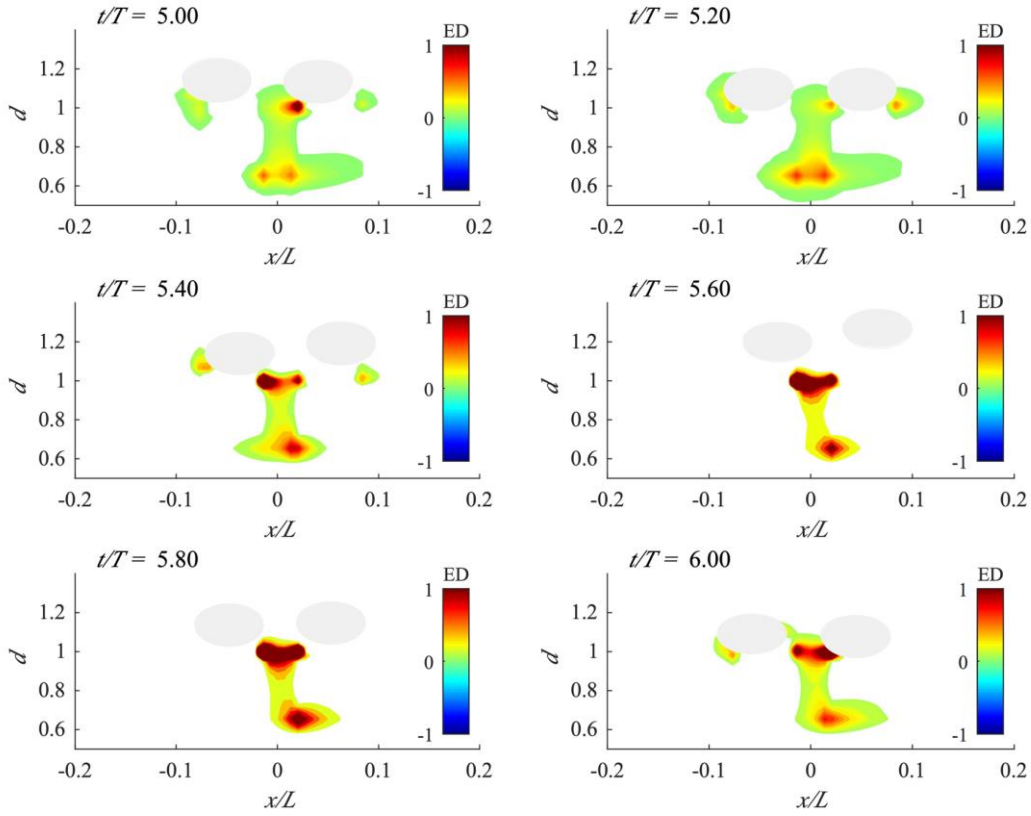

Figure 9. Instantaneous position of optimum TPFB in a characteristic pattern of energy dissipation for one wave cycle (T = 1.4 s).

CONCLUSIONS

The integrated modelling approach is applied in the present multi-objective optimization study on the fishing net porosity attached between twin pontoons of a floating breakwater (TPFB) using genetic algorithm (GA) and computational fluid dynamic (CFD) model. The numerical model is based on the extended Reynolds Average Navier-Stokes (RANS) solver for solid-permeable obstacle with turbulence closure model, and the volume of fluid (VOF) method. The effects of selected porosities, n ratios were examined accordingly at various wave heights and periods to produce significant results of hydrodynamic coefficients in a complete numerical optimization simulation. The optimum result was chosen from various populations and generations, in which it is then quantified qualitatively by some visualizations on the characteristic pattern of induced energy dissipation. The results are concluded as follows:

- The capability of the numerical model has been demonstrated, in which the numerical results agree fairly well with measurements. The numerical results show a significant correlation between the environmental tested conditions and the characteristics of K_t, as well motion responses of TPFB.
- Besides that, the robustness of the numerical GA computation has been clearly demonstrated by optimizing the fishing net porosity, n subjected to multiple objectives and constraints on the hydrodynamic coefficients consist of K_t, K_r and K_d towards obtaining an optimum hydrodynamic performance of TPFB.
- In particular, the optimum porosity results in the enhancement of K_d approximately greater than 0.34, while leading to decrements in K_t and K_r approximately less than 0.85 and 0.42 respectively, which are found to be consistent with derived algebraic expressions of the fishing net model.
- In corresponding to the characteristics of K_t, K_r and K_d, the CFD result showed that the optimum TPFB leads to a further increment in the wave absorbing effect associated with turbulence energy dissipation, as compared to the existing one, which is still currently has been difficult to measure using experiments.
- Further improvements in terms of problem variables and objectives are suggested to enhance the optimization approach, in which the effects of irregular wave, current velocity, and a number of fishing net layers are among the next steps to be incorporated in optimization algorithm.
- More validations on the hydrodynamic performance of the optimized porosity of TPFB including shoreline response are necessarily needed, for instance; quantifying sediment scour at beach-breakwater distance [15]. This can be made using primary data or secondary data taken from experimental and numerical studies.

ACKNOWLEDGMENTS

The authors would like to thank and express their great appreciation to Universiti Malaysia Terengganu for its support in the completion of this research.

REFERENCES

[1] S. F. Abdullah and A. Fitriadhy, "Application of genetic algorithm for optimum hydrodynamic performance of twin pontoon floating breakwater," *J. Water., Port, Coast. Ocean Eng.*, vol. 146, no. 2: 04019040, 2020, doi: 10.1061/(ASCE)WW.1943-5460.0000548.

[2] G. Elchahal, P. Lafon and R. Younes, "Design optimization of floating breakwaters with an interdisciplinary fluid–solid structural problem." *Can. J. Civ. Eng.*, vol. 36, no. 11, pp. 1732–1743, 2009, doi: 10 .1139/L09-095.

[3] F. Mahmuddin and M. Kashiwagi, "Design optimization of a 2D asymmetric floating breakwater by genetic algorithm," in *Proc., 22 Int. Offshore and Polar Engineering*, pp. 1263–1270, 2012.

[4] G. Elchahal, R. Younes and P. Lafon P, "Optimization of coastal structures: application on detached breakwaters in ports," *Ocean Eng.*, vol. 63, pp. 35-43, 2013, doi: 10.1016/j.oceaneng.2013.01.021.

[5] N. Abdussamie, R. Ojeda and M. Daboos. "ANFIS method for ultimate strength prediction of unstiffened plates with pitting corrosion," *Ships Offs. Struc.*, vol. 13, no. 5, pp. 540-550, 2018.

[6] H. Azimi, H. Bonakdari, I. Ebtehaj, S. Shabanlou, S. H. A. Talesh, and A. Jamali, "A pareto design of evolutionary hybrid optimization of ANFIS model in prediction abutment scour depth," *S ̄adhan ̄a*, vol. 44, no. 169, pp. 1-14, 2019, doi: 10.1007/s12046-019-1153-6.

[7] M. Gaber, S. El-Banna, M. El-Dabah and M. Hamad, "Designing and implementation of an intelligent energy management system for electric ship power system based on adaptive neuro-fuzzy inference system (ANFIS)," *Adv. Sci., Tech. Eng. Sys. J.*, vol. 6, no. 2, pp. 195-203, 2021.

[8] K. Wang, X. Yan, Y. Yuan and D. Tang, "Optimizing ship energy efficiency: application of particle swarm optimization algorithm," *Proc., Ins. Mech. Eng. Part M: J. Eng. Maritime Env.*, vol. 232, no. 4, pp. 379-391, 2018, doi: 10.1177/1475090216638879.

[9] S. L. Zhang, B. J. Zhang, T. Tezdogan, L. P. Xu, and Y. Y. Lai, "Research on bulbous bow optimization based on the improved PSO algorithm," *China Ocean Eng.*, vol. 31, no. 4, pp. 487-494, 2017.

[10] S. O. Fadlallah, T. N. Anderson and R. J. Nates, "Artificial neural network–particle swarm optimization (ANN-PSO) approach for behaviour prediction and structural optimization of lightweight sandwich composite heliostats," *Arab. J. Sci. Eng.*, pp. 1-22, 2021.

[11] X. Jialing, S. Weifeng, B. Zong and S. Tiewei, "Research on marine electric load forecast based on PSO-Elman neural network," in *2021 4th Int. Conf. E., Elec. Pow. Eng. (CEEPE)*, IEEE,, pp. 1220-1224, 2021.

[12] ITTC, "Uncertainty analysis in CFD verification and validation methodology and procedures-ITTC-Recommended Procedures and Guidelines 7.5-03-01-01," in *Proc., 28th Int. Tow. Tank Conf.*, Wuxi China, 2017.

[13] C-Y Ji, X. Chen, J. Cui, Z-M Yuan and A. Incekik, "Experimental study of a new type of floating breakwater," *Ocean Eng.*, vol. 105, pp. 295-303, 2015, doi: 10.1016/j.oceaneng.2015.06.046

[14] A. Fitriadhy, S. F. Abdullah, M. hairil, M. F. Ahmad and A. Jusoh, "Optimized modelling on lateral separation of twin pontoon-net floating breakwater," *J. Mech. Eng. Sci.*, vol. 13, no. 4, pp. 5764-5779, 2019, doi: 10.15282/jmes.13.4.2019.04.0460.

[15] A. Fitriadhy, M. A. Faiz and S. F. Abdullah, "Computational fluid dynamics analysis of cylindrical floating breakwater towards reduction of sediment transport," *J. Mech. Eng. Sci.*, vol. 11, no. 4, pp. 3072-3085, 2017, doi: 10.15282/jmes.11.4.2017.10.0276.